

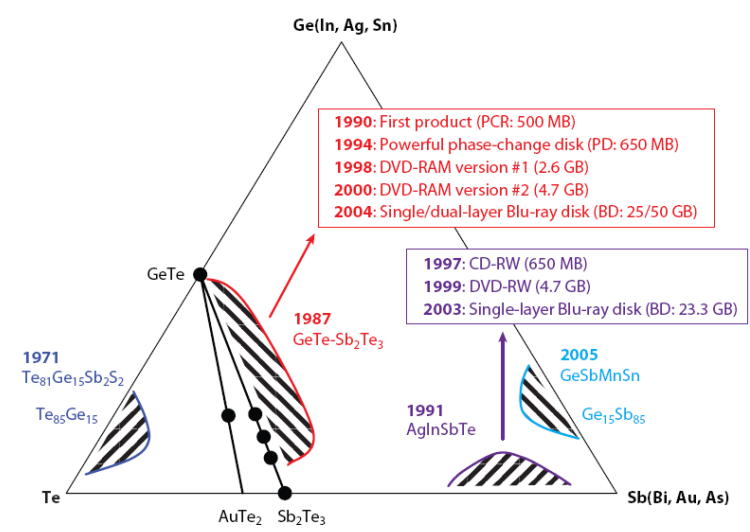
Electronics applications II



- ✓ Structure of fast-phase-change chalcogenides
 - Crystalline structures and related properties
 - Structures of the amorphous phase
- ✓ Prospects and opportunities from the material's viewpoint

Phase change materials; structural aspects

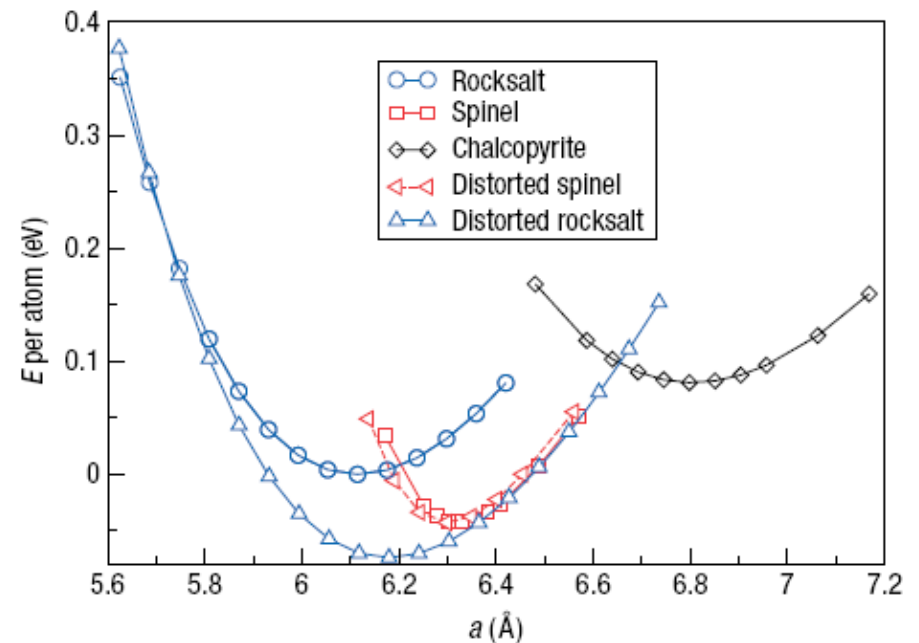
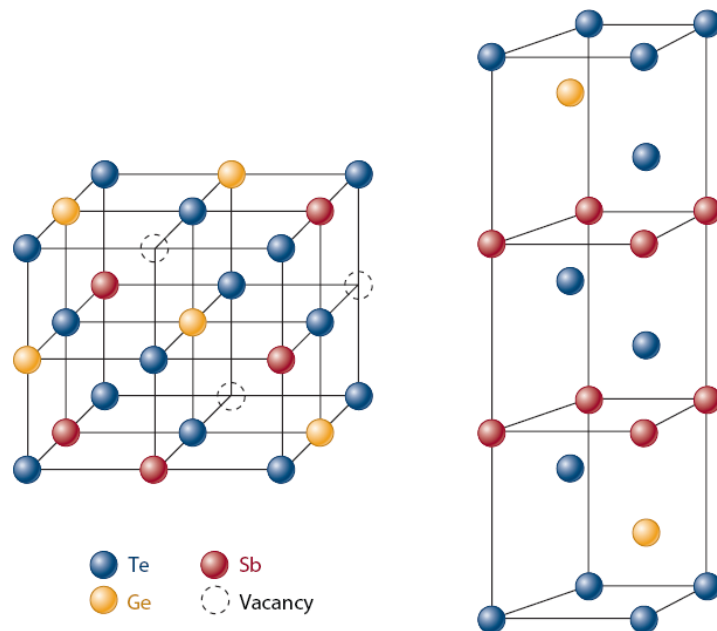
- ✓ **The crystalline side of the phase change chalcogenides is being revealed rapidly.**
 - Only a certain family of crystalline structures seem to be suitable.
 - Only specific chemical bonds, thus atomic combinations, seem to be allowed.
 - Very high dielectric constant and disorder-driven (Anderson-type) MIT
- ✓ **The amorphous side of the phase change chalcogenides is relatively not known.**
 - Lack of good experimental probes for structural analysis
 - Diverse structural parameters, sometimes contradictory each other
- ✓ **Some related questions not clearly answered yet;**
 - How and why are the amorphous phases stable despite the fast crystallization?
 - Are the amorphous structures of PCM very different from those of typical ChGs?
 - Can the concepts and languages of traditional ChGs be also applied?
 - What amorphous structure(s) is most suitable as phase change materials?
 - What is the origin(s) of threshold switching?
 - What are the traps of charge carriers?
 - What is the next question?



Drawing taken from Wuttig and Yamada, Nat. Mater. 6 (2007) 824.

Crystal structure of GST

- ✓ In general, the most successful (fastest-switching) PCMs show a simple cubic or a (distorted) rocksalt structure, often with random occupation of the lattice sites by the atoms composing the alloy.
- ✓ Crystalline GST-225 is formed at $\sim 140^\circ\text{C}$, depending on the heating rate.
- ✓ Te atoms occupy one FCC sublattice, while Ge, Sb, and a relatively large amount of vacancies ($\sim 20\%$) randomly occupy the other sublattice.
- ✓ At $\sim 310^\circ\text{C}$, more stable hexagonal phase is formed.

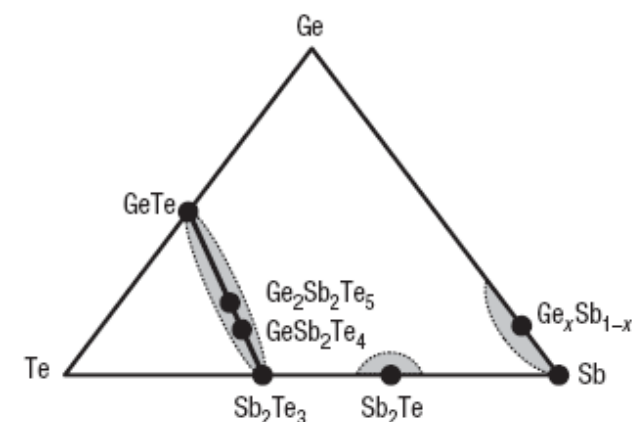


Welnic et al, Nat. Mater. 5 (2006) 56.

Raoux, Annu. Rev. Mater. Res. 39 (2009) 25.

Crystal structure of PCMs

Material	Structure	Average number of valence electrons
Successful samples*		
GeTe	Rocksalt	5
Ge ₁ Sb ₂ Te ₄	Rocksalt (metastable)	4.75
Ge ₂ Sb ₂ Te ₅	Rocksalt (metastable)	4.8
Ge ₄ Sb ₁ Te ₅	Rocksalt	5.1
In ₃ SbTe ₂	Rocksalt	4.33
AgSbTe ₂	Rocksalt	4.5
AuSbTe ₂	Rocksalt	4.5
Au ₂₅ Ge ₄ Sn ₁₁ Te ₆₀	Cubic	4.45
Ag ₃ In ₄ Sb ₇₆ Te ₁₇	Cubic	4.93
Ag _{5.5} In _{6.5} Sb ₅₉ Te ₂₉	Cubic-like/hexagonal	4.94
Unsuccessful samples		
AgInTe ₂	Chalcopyrite	4
AuInTe ₂	Chalcopyrite	4



*Success is defined as the existence of a significant difference in the dielectric function of the amorphous and crystalline state ensuring optical contrast. Note that Ge₁Sb₂Te₄ and Ge₂Sb₂Te₅ each have one vacancy per unit cell in the cubic structure.

Resonant bonding of crystalline PCMs

- ✓ Infrared reflectance spectra of several PCM films reveal significant discrepancy in optical properties between amorphous and crystalline phases.

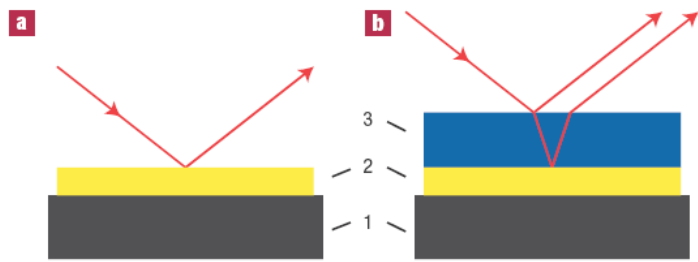


Figure 1 Sample cross-section. a, Reference specimen. b, Sample investigated. 1: glass substrate, 2: Au layer, 3: semiconductor layer.

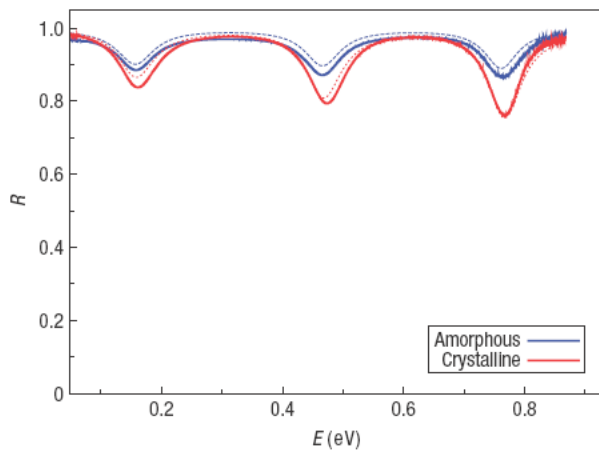


Figure 2 Infrared reflectance spectra of an AgInTe_2 film with a thickness of $0.65 \mu\text{m}$. Blue: amorphous state, red: crystalline state. The solid lines describe the experimental data, whereas the dashed lines denote the simulation results.

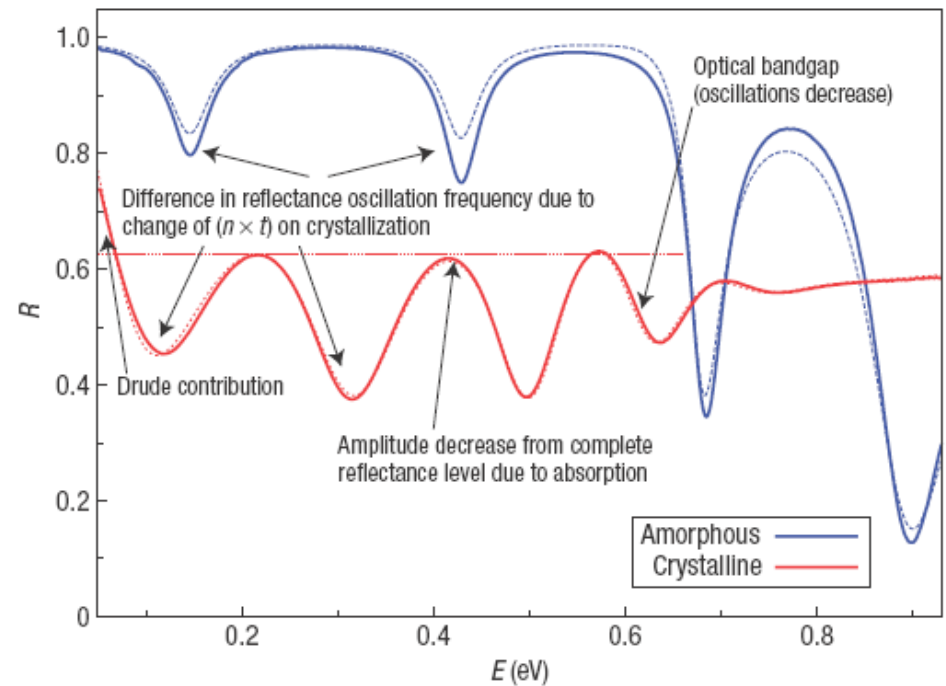


Figure 3 Infrared reflectance spectra of a $\text{Ge}_2\text{Sb}_1\text{Te}_4$ film. Blue: amorphous state, red: crystalline state. The solid lines describe the experimental data, whereas the dashed lines denote the simulation results. On crystallization, the thickness decreased from 0.53 to $0.50 \mu\text{m}$. The contributions of different phase-change film properties to the reflectance curve are marked.

Resonant bonding of crystalline PCMs

- ✓ The crystal structures of PCMs are all based on distorted cubic structures and all possess resonant bonding which is the cause of their higher optical dielectric constants.
- ✓ Resonant bonding requires a longer-range order than the conventional electron pair bond of the 8-*N* rule. In the amorphous state, the structure seems to revert to a simple 8-*N* rule structure.

Table 1 Optical dielectric constants and energy gaps. This table comprises the measured optical dielectric constants ϵ_∞ of amorphous and crystalline phases of phase-change materials without Drude contribution, and Se, Te (refs 24,25). In addition, on the right-hand side the optical gaps E_g are listed. The third column is a measure of resonance bonding in the crystalline state. AIST: $\text{Ag}_5\text{In}_6\text{Sb}_{59}\text{Te}_{30}$.

	ϵ_∞			E_g		
	Amorphous	Crystalline	% increase	Amorphous	Crystalline	% decrease
$\text{Ge}_1\text{Sb}_2\text{Te}_4$	16.6 ± 0.3	36.2 ± 0.9	118	0.76	0.39	49
$\text{Ge}_1\text{Sb}_1\text{Te}_2$	14.8 ± 0.4	47.7 ± 0.8	222	0.77	0.20	74
GeTe	13.2 ± 0.2	33.2 ± 0.8	152	0.78	0.55	35
$\text{Ge}_2\text{Sb}_2\text{Te}_5$	16.0 ± 0.4	33.3 ± 0.8	108	0.77	0.48	29
$\text{Ge}_{15}\text{Sb}_{85}$	26.9 ± 0.7	—	—	0.41	—	—
$\text{Ge}_2\text{Sb}_1\text{Te}_4$	14.5 ± 0.3	29.8 ± 1.6	106	0.80	0.61	24
$\text{Ge}_3\text{Sb}_4\text{Te}_8$	15.6 ± 0.2	43.4 ± 1.2	178	0.79	0.24	70
AIST	19.6 ± 0.5	52.8 ± 1.5	169	0.63	0.18	71
Te	11	33.4	204			
Se	5.7	9.79	72			

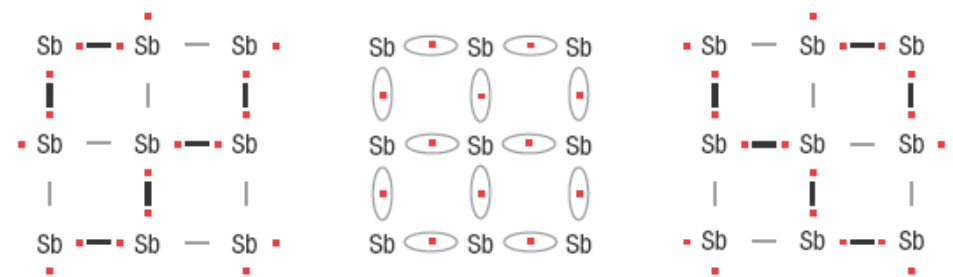


Figure 5 Schematic diagram demonstrating the origin of resonance bonding for Sb. On the left-hand side, one limiting case for bonding in an undistorted Sb phase is shown. A second limiting case is shown on the right-hand side. The solid can minimize its energy by forming a hybrid wavefunction, which is shown in the middle of this figure. This bonding is described as resonance bonding. The pronounced electron delocalization gives rise to an increased electronic polarizability.

Resonant bonding of crystalline PCMs

- ✓ The degree of ionicity and the tendency towards hybridization of the bonding.
- ✓ A map is spanned by two coordinates of these two quantities that can be calculated from the composition.

$$r'_\sigma = r_p^A - r_p^B,$$

$$r_\pi^{-1} = [(r_p^A - r_s^A) + (r_p^B - r_s^B)]^{-1}.$$

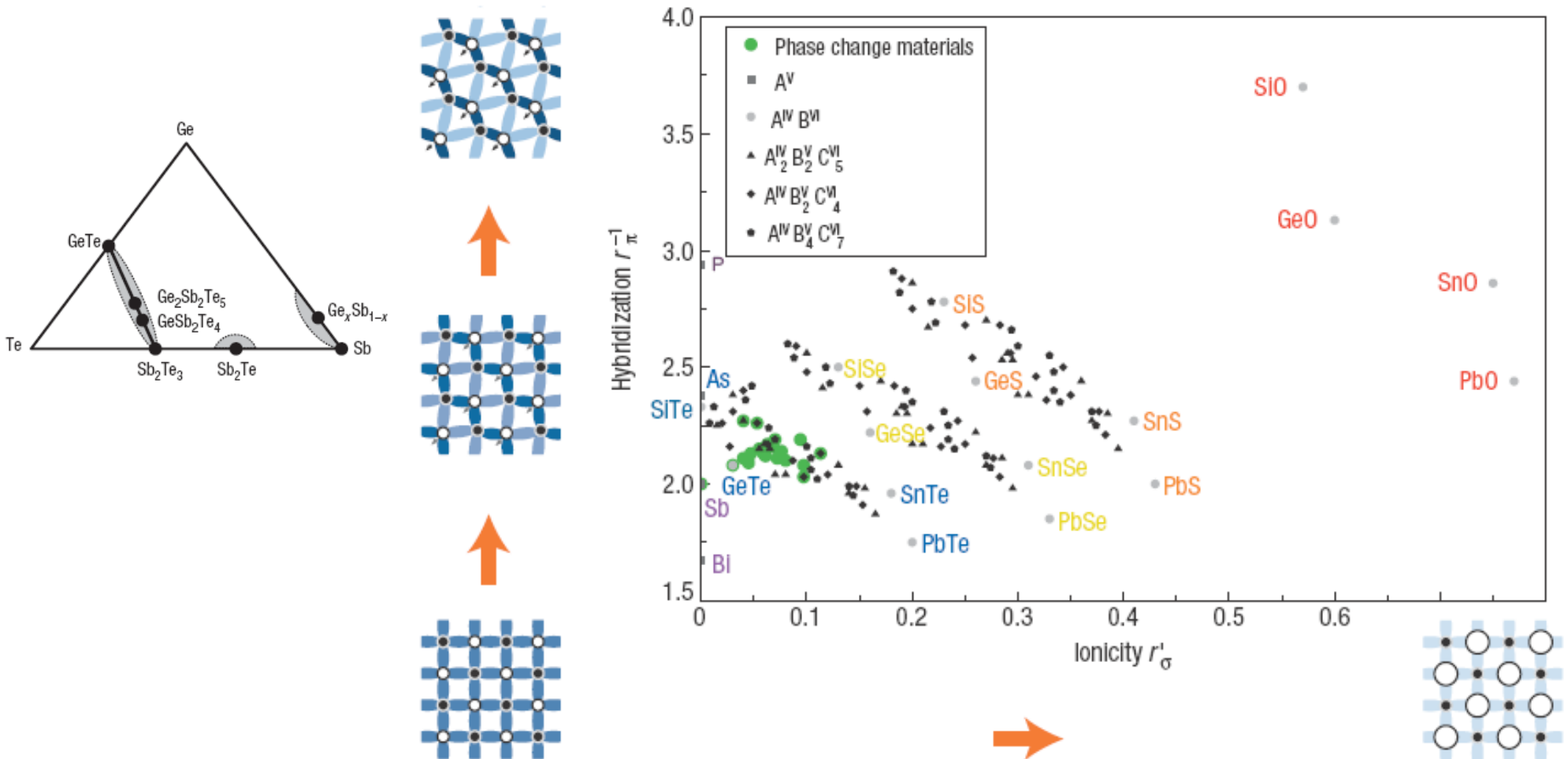
Here, r_s^X and r_p^X denote the valence radii of the s - and p -orbital of atom X , respectively. The coordinate r'_σ provides a quantitative measure for the ionicity of bonds similar to Pauling's electronegativity difference. The second coordinate r_π^{-1} describes the degree of 'covalency'. It can be understood as a measure of the energetic splitting of s - and p -states, which scales with the difference between the radii of s - and p -orbitals. Littlewood coined the term covalency for this quantity; however, we prefer to call it 'tendency towards hybridization' or just 'hybridization' instead. For

$$r'_\sigma = \underbrace{\left(\frac{\sum_i n_i r_{p,i}}{\sum_i n_i} \right)}_{\text{Anions}} - \underbrace{\left(\frac{\sum_j n_j r_{p,j}}{\sum_j n_j} \right)}_{\text{Cations}},$$

$$r_\pi^{-1} = \left[\underbrace{\left(\frac{\sum_i n_i (r_{p,i} - r_{s,i})}{\sum_i n_i} \right)}_{\text{Anions}} + \underbrace{\left(\frac{\sum_j n_j (r_{p,j} - r_{s,j})}{\sum_j n_j} \right)}_{\text{Cations}} \right]^{-1}$$

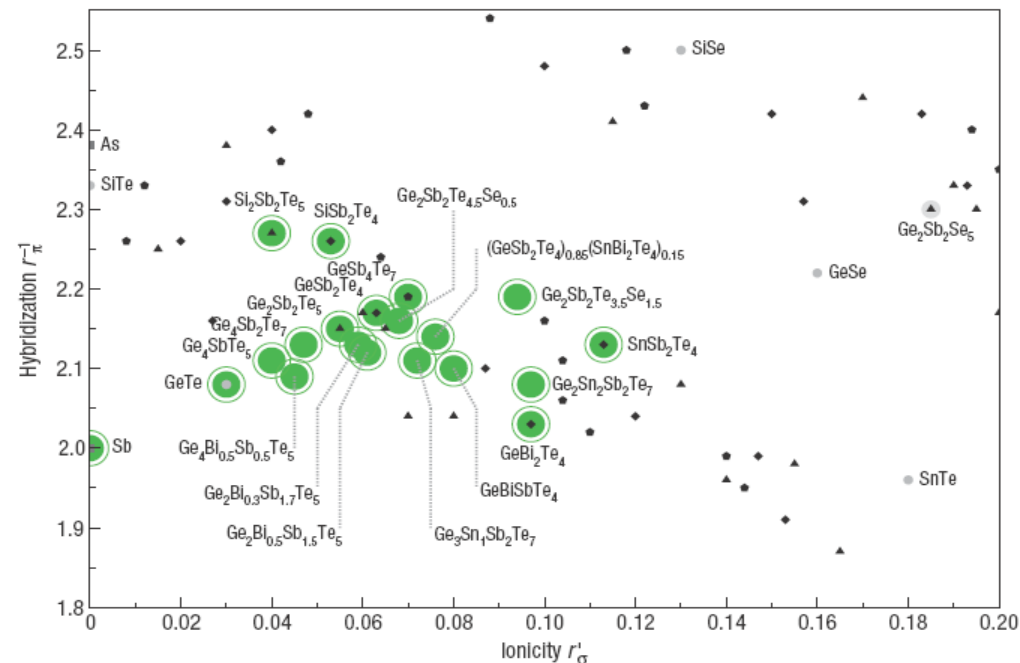
Resonant bonding of crystalline PCMs

- ✓ PCMs are located at relatively well-defined narrow region that is an inherent characteristic of PCMs.



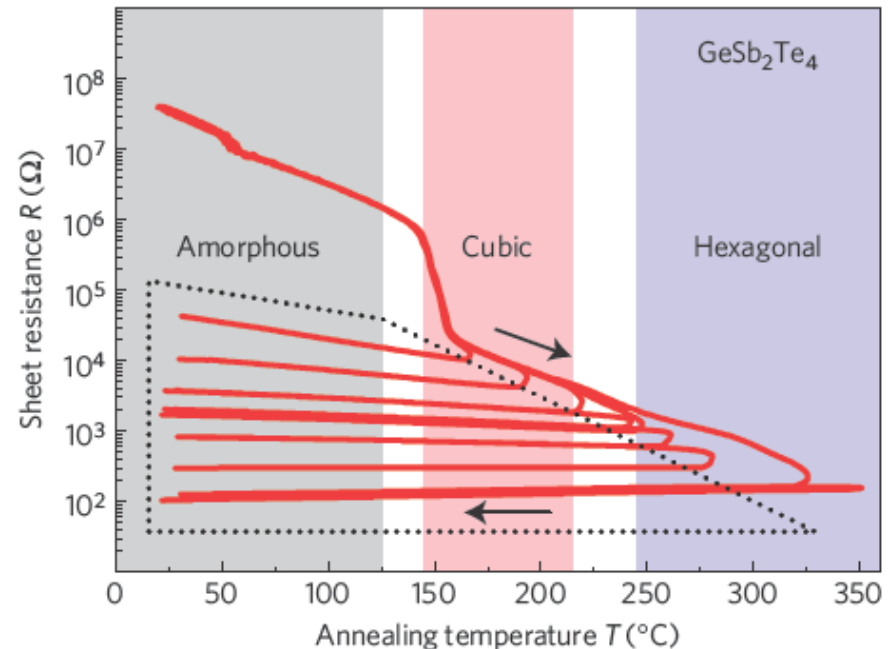
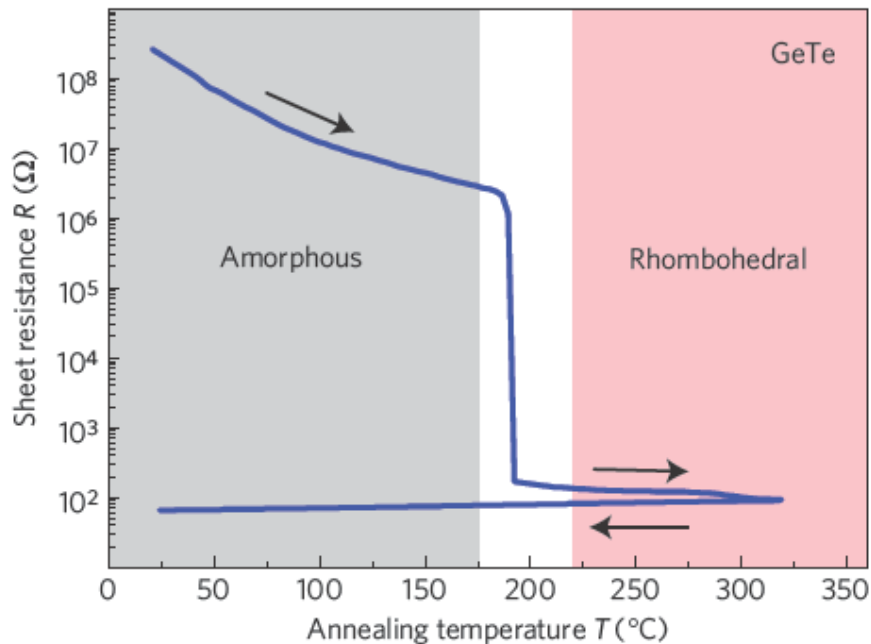
Resonant bonding of crystalline PCMs

- ✓ The resonance character is weakened both by increasing hybridization as well as increasing ionicity.
- ✓ Increasing the hybridization leads to larger distortions that favor a smaller number of more saturated covalent bonds.
- ✓ Increasing ionicity also reduces resonant bonding because the charge is increasingly localized at the ion cores.
- ✓ The region for PCMs is characterized by the pronounced resonance bonding in the crystalline state.



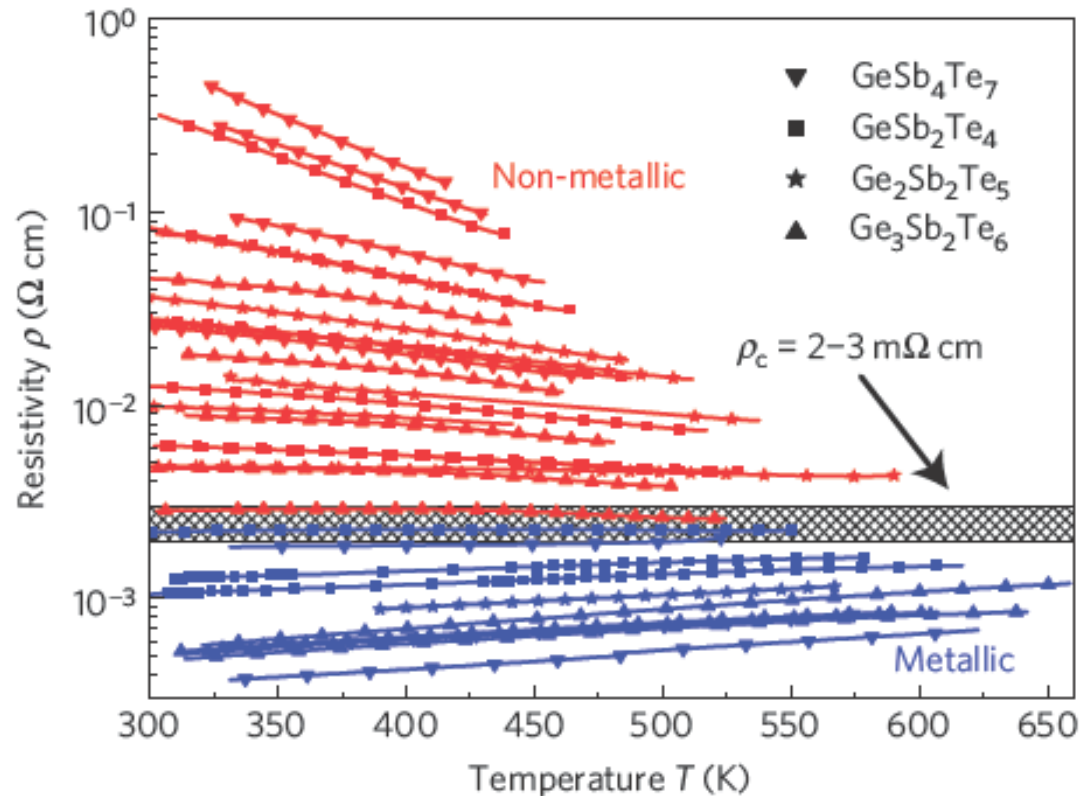
Disorder-induced MIT in crystalline PCMs

- ✓ Temperature dependence of the sheet resistance of a GeTe film (left) and a GST-124 film (right) on heating and subsequent cooling to room temperature.
- ✓ The crystallization of the initially amorphous GeTe film at 192C into the crystalline phase is accompanied by a distinct drop of resistivity.
- ✓ The crystalline GeTe phase shows a $TCR > 0$ with no changes on annealing.
- ✓ The room-temperature resistance of crystalline GST-124 decreases by a factor of approximately 400 on increasing the annealing temperature from 150 to 350C.
- ✓ The change from non-metallic ($TCR < 0$) to metallic ($TCR > 0$) behavior occurs with increasing annealing temperature.



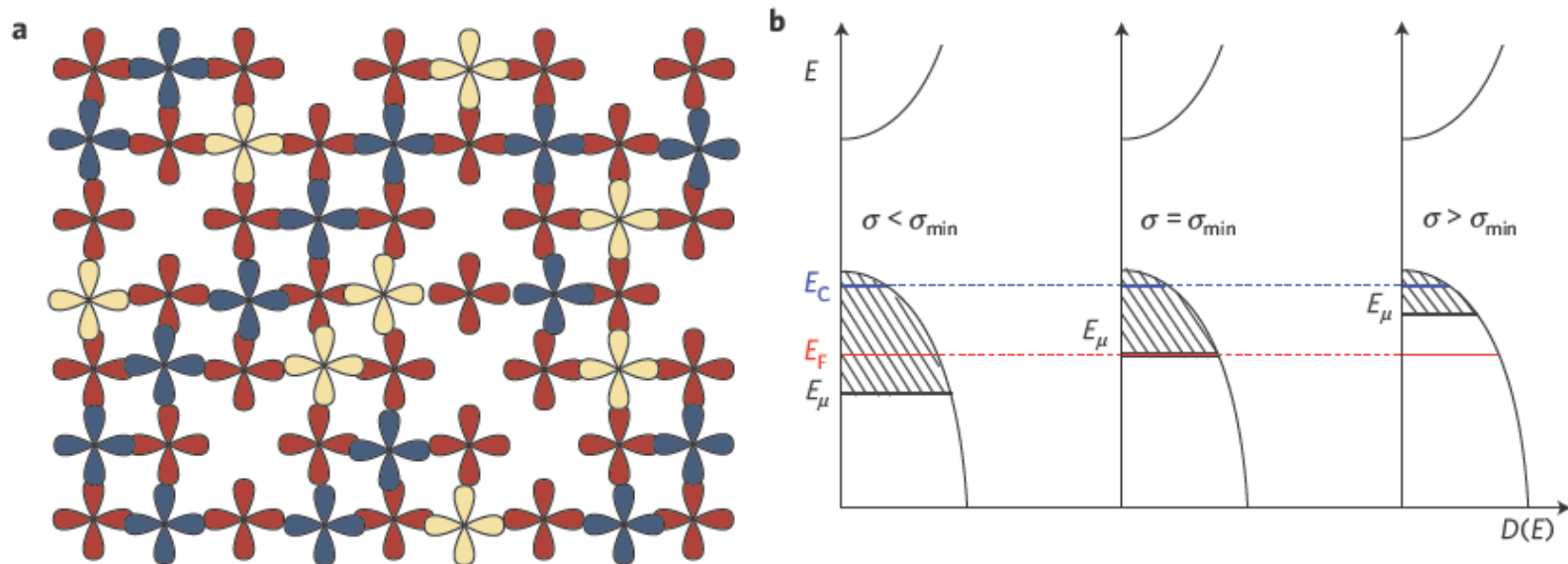
Disorder-induced MIT in crystalline PCMs

- ✓ With increasing annealing temperature a systematic change of the resistivity and TCR is observed for four different GeSbTe alloys.
- ✓ At a critical resistivity of about 2-3 mΩcm, the behavior changes from non-metallic ($d\rho/dT < 0$) to metallic behavior ($d\rho/dT > 0$) for all four alloys, indicative of a universal MIT on annealing.



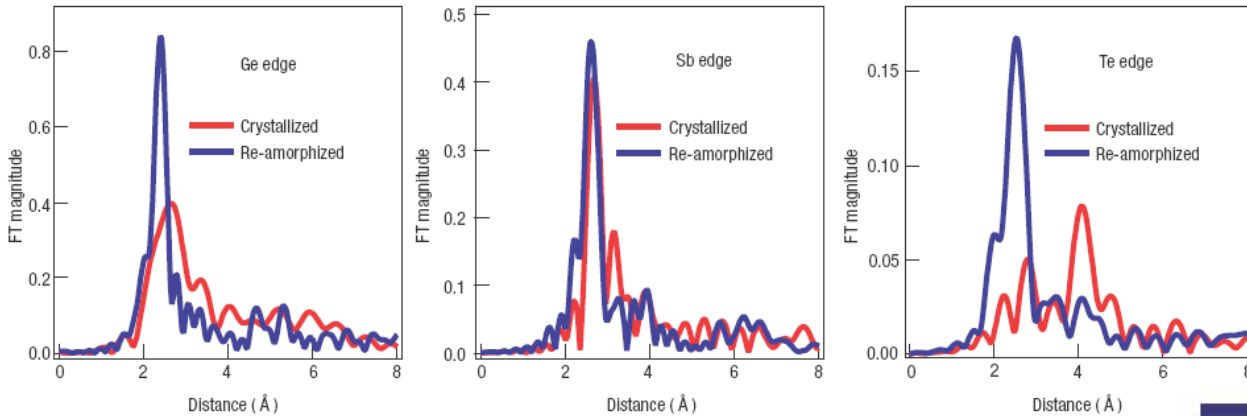
Disorder-induced MIT in crystalline PCMs

- ✓ Structure of GST-124 shows that the anion sublattice is occupied with Te atoms (red) whereas the cation sublattice is randomly occupied with Ge atoms, Sb atoms (light yellow and blue, respectively) and empty lattice sites.
- ✓ The random occupation in combination with distortions leads to tremendous variations of the atomic orbitals' overlap, giving rise to pronounced disorder-related effects on the band structure.
- ✓ As long as the Fermi energy E_F lies within the localized states (shaded regions) the system is insulating (left). Annealing reduces the disorder and thus lifts the mobility edge E_μ . When the mobility edge passes the Fermi energy (centre) the 'Anderson-like' transition to metallic behavior (right) occurs.



Amorphous structures proposed

- ✓ EXAFS analysis for crystalline and laser-amorphized states.
- ✓ The umbrella flip of Ge atoms is proposed for fast diffusionless crystallization.



Bond	Bond length (Å)	
	From EXAFS	From XRD
Crystallized state		
Ge-Te	2.83 ± 0.01	$3.0(1) \pm 0.3$
Sb-Te	2.91 ± 0.01	$3.0(1) \pm 0.3$
Te-Te (2nd)	4.26 ± 0.01	$4.2(6) \pm 0.2$
Laser-amorphized state		
Ge-Te	2.61 ± 0.01	2.61*
Sb-Te	2.85 ± 0.01	

*Calculated based on the rocksalt lattice parameter assuming Ge atoms occupy tetrahedrally coordinated sites in the Te f.c.c. sublattice

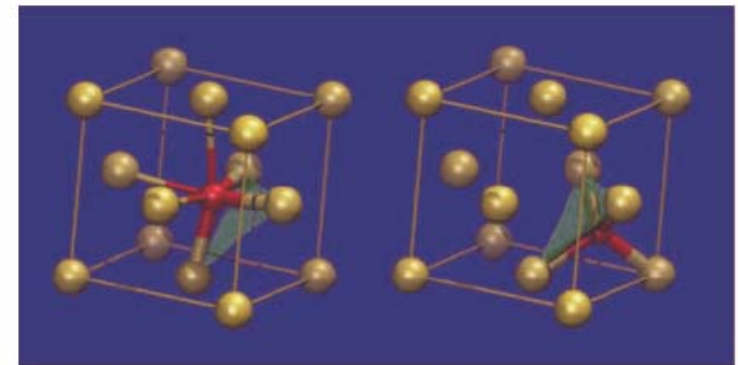
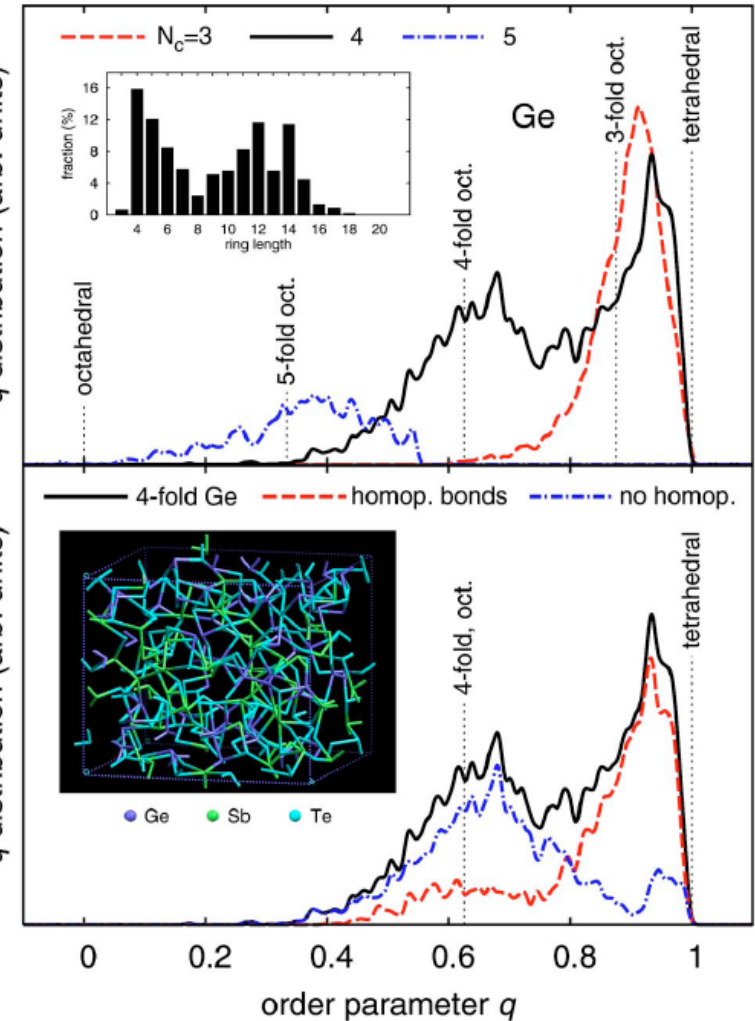


Figure 5 Fragments of the local structure of GST around Ge atoms in the crystalline (left) and amorphous (right) states. Stronger covalent bonds are shown as thicker lines whereas weak interblock bonds are shown as thinner lines. Notice that the stronger covalent bonds remain intact on the umbrella-flip structural transformation rendering the Ge sublattice random. It is this nature of the structural change that makes the medium fast and stable.

Amorphous structures proposed

- ✓ On the structure of amorphous GST-225, *ab initio* molecular dynamics simulations were done.
- ✓ One third of Ge atoms are in a tetrahedral environment while the remaining Ge, Sb, and Te atoms display a defective octahedral environment, reminiscent of cubic crystalline GST.
- ✓ (Top panel) distribution of Ge with different coordination number.
- ✓ (Bottom panel) : distribution of four-coordinated Ge with at least one homopolar bond with Ge or Sb, or bonding with Te.



Average coordination number				
	With Ge	With Sb	With Te	Total
Ge	0.275	0.270	3.277	3.823
Sb	0.270	0.588	3.166	4.025
Te	1.311	1.267	0.288	2.866

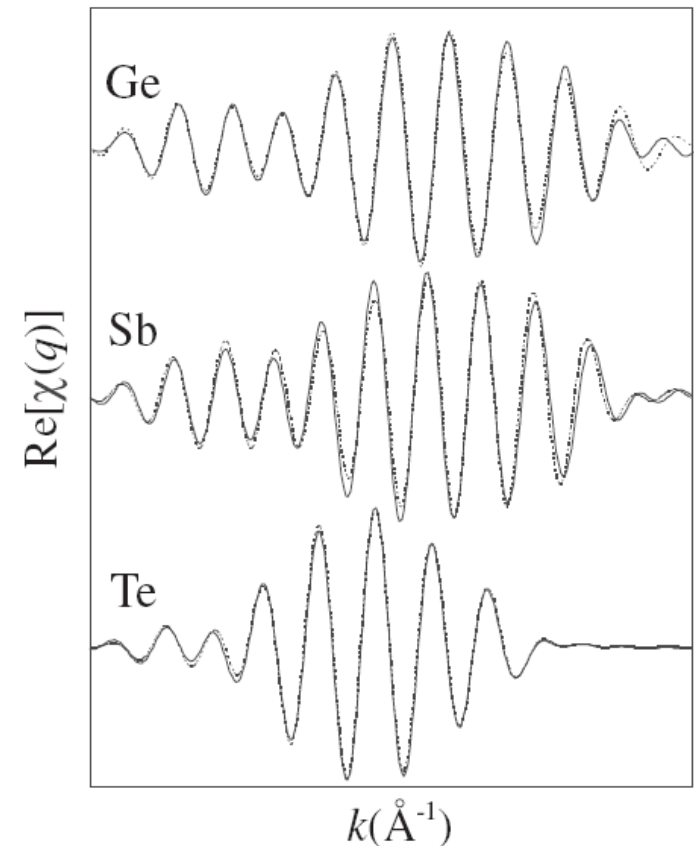
Amorphous structures proposed

- ✓ EXASFS analysis carried out with amorphous GST-225.
- ✓ Application of the bond constraint theory indicates that the amorphous phase is an ideal network structure in which the average number of constraints per atom equals the network dimensionality, 3.

The total number of constraints for the entire $\text{Ge}_2\text{Sb}_2\text{Te}_5$ alloy follows: Ge contribution: $4.33 \times 2 = 8.66$; Sb contribution: $4.5 \times 2 = 9$; Te contribution: $2 \times 5 = 10$. Thus,

$$C_{\text{av}} = \frac{8.66 + 9 + 10}{9} = 3.07.$$

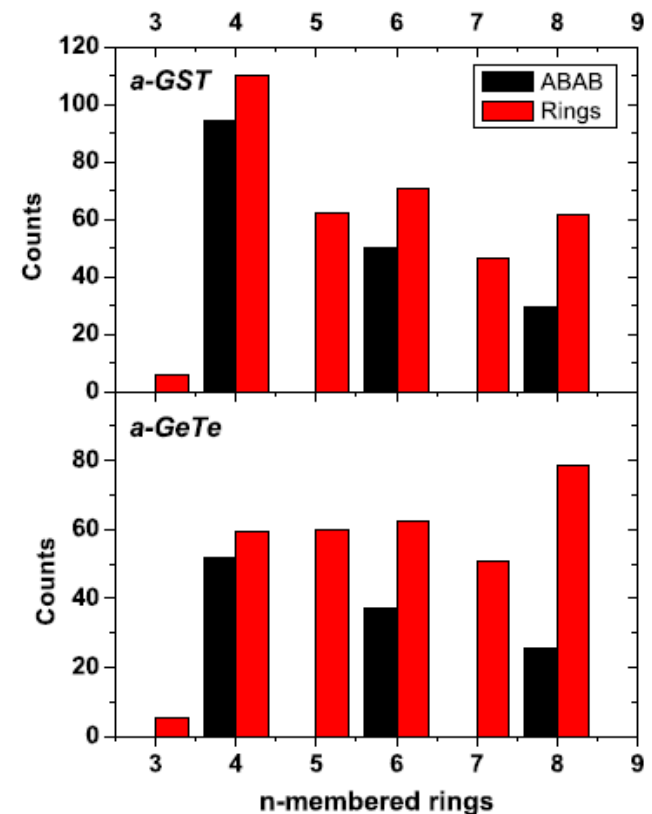
Atom	Bond	Coordination	R (Å)
Ge	Ge-Te	3.3 ± 0.5	2.63 ± 0.01
	Ge-Ge	0.6 ± 0.2	2.47 ± 0.03
Sb	Sb-Te	2.8 ± 0.5	2.83 ± 0.01
	Te-Ge	1.2 ± 0.3	2.62 ± 0.01
Te	Te-Sb	1.2 ± 0.3	2.83 ± 0.01



Amorphous structures proposed

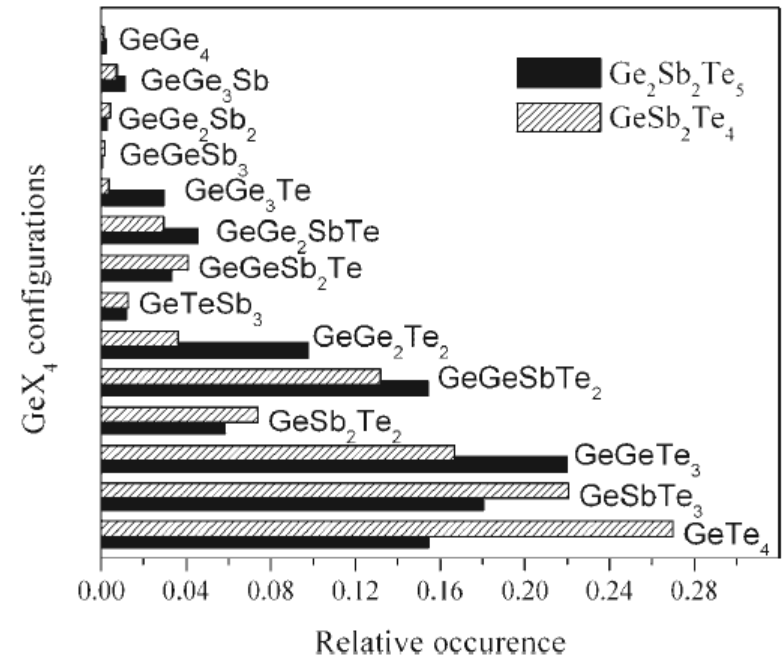
- ✓ Density functional simulations carried out on GST-225.
- ✓ There are deviations from the 8-N rule for CN, with Te having near threefold coordination. Ge atoms are predominantly fourfold coordinated, but in only about one-third of the Ge atoms. The average CN of Sb atoms is 3.7, and the local environment of Ge and Sb is usually distorted octahedral.
- ✓ There is crucial structural motif which is a four-membered ring with alternating atoms of types, ABAB square. The rapid phase change is a reorientation of disordered ABAB squares to form an ordered lattice.

	<i>a</i> -Ge ₂ Sb ₂ Te ₅		<i>c</i> -Ge ₂ Sb ₂ Te ₅	
	Calculated	Expt.	Calculated	Expt.
r_0 (Å)	2.78/2.93	2.61/2.85 ^a 2.63/2.83 ^c	2.92/3.02	2.83/2.91 ^a 3.0±0.3 ^a
r_{min} (Å)	3.84/3.88			
n_{Ge}	4.2	3.9±0.8 ^c		6
n_{Sb}	3.7	2.8±0.5 ^c		6
n_{Te}	2.9	2.4±0.8 ^c		4.8 ^d
α_{Ge}	0.77			1
α_{Sb}	0.61			1
α_{Te}	0.75			1
V_v (%)	11.8			~10



Amorphous structures proposed

- ✓ The amorphous structure GST-225 and -124 was investigated by XRD, EXAFS, and neutron diffraction. Then, the reverse Monte Carlo simulation technique was used to generate large scale atomic models compatible with all experimental data sets.
- ✓ The homopolar Ge-Ge bonding is present already in -124, and significant Ge-Sb bonding in both compositions.
- ✓ All atomic species satisfy formal valence requirements: the 8-*N* rule.
- ✓ The predominance of GeTe_4 or $\text{Te}_3\text{Ge-GeTe}_3$ units in these compositions can be excluded. Instead, these alloys are characterized by a variety of local motifs.



Alloy	Parameter	Te-Sb	Te-Ge	Sb-Ge	Ge-Ge	Te-X	Sb-X	Ge-X
Ge ₂ Sb ₂ Te ₅	r_{ij}	2.82	2.60	2.69	2.48			
	N_{ij}	1.01	0.98	0.60	0.79	1.99	3.12	3.85
GeSb ₂ Te ₄	r_{ij}	2.83	2.61	2.69	2.48			
	N_{ij}	1.29	0.69	0.33	0.49	1.98	2.91	3.91

Amorphous structures proposed

- ✓ To determine the crystalline and amorphous structures of AIST and how they differ from GST, XRD, EXAFS and XPS experiments with density functional simulations are carried out.

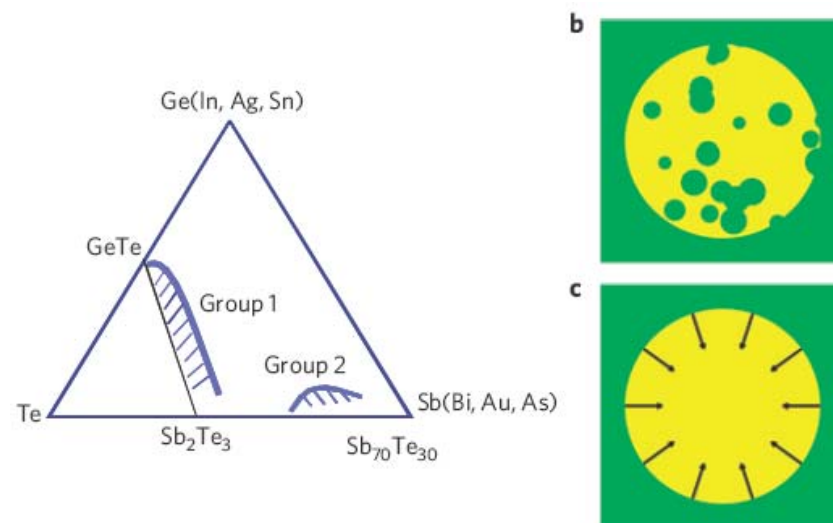


Table 1 | Local structure of a-AIST determined by EXAFS at 26 K and DF-MD calculations.

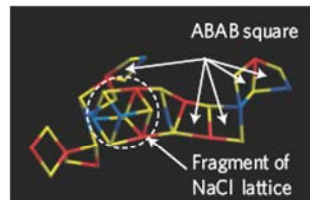
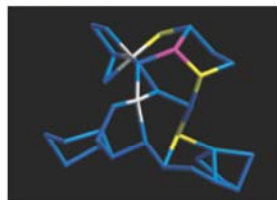
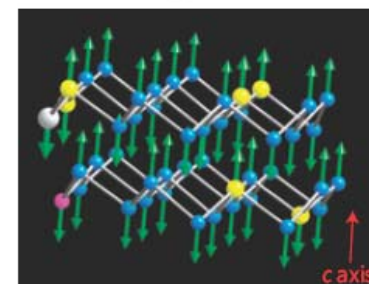
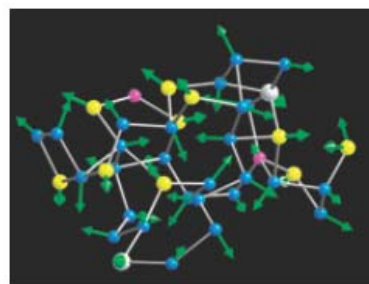
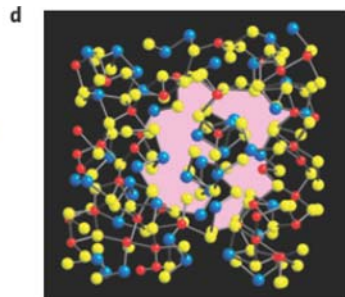
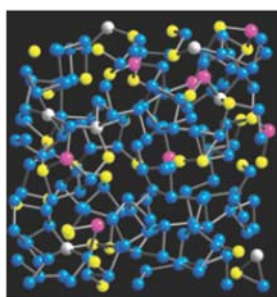
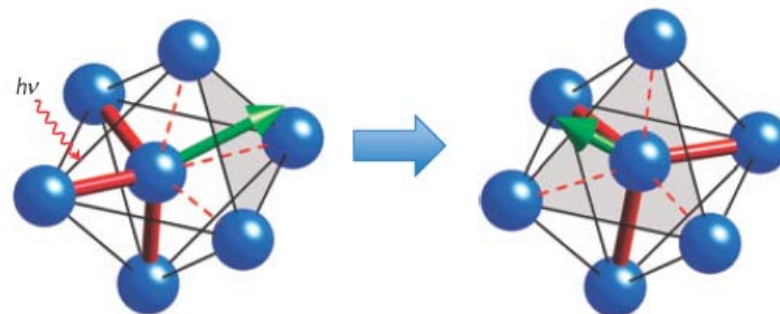
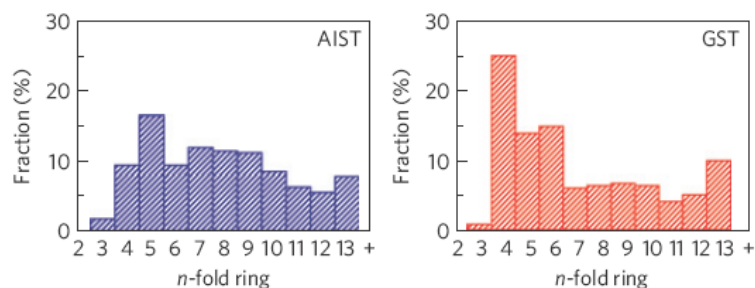
Atom (<i>i</i>)	N_{EXAFS}	r_{EXAFS} (Å)	$N_{\text{DF-MD}}$	$r_{\text{DF-MD}}$ (Å)	N_{bond}
Ag	3.3 ± 0.5	2.768 ± 0.006	4.4	2.80 ± 0.05	1.9 (2.0)
In	4.3 ± 0.6	2.826 ± 0.006	3.1	2.85 ± 0.05	2.5 (2.9)
Sb	3.7 ± 0.3	2.872 ± 0.006	3.3	2.85 ± 0.05	3.1 (3.2)
Te	2.4 ± 0.4	2.827 ± 0.006	2.5	2.85 ± 0.05	2.5 (2.6)

N , coordination number; r , nearest-neighbour bond length; N_{bond} , chemical coordination number. Theoretical values from RMC-refined DF geometry ($N_{\text{DF-MD}}$ and $r_{\text{DF-MD}}$) and chemical bond-order analysis. The N_{bond} values of c-AIST are given in parentheses. Supplementary Table S1 provides more information on $N_{\text{DF-MD}}$ and $r_{\text{DF-MD}}$.

* The chemical coordination numbers are calculated by adding the bond orders to the coordination numbers for individual atoms.

Amorphous structures proposed

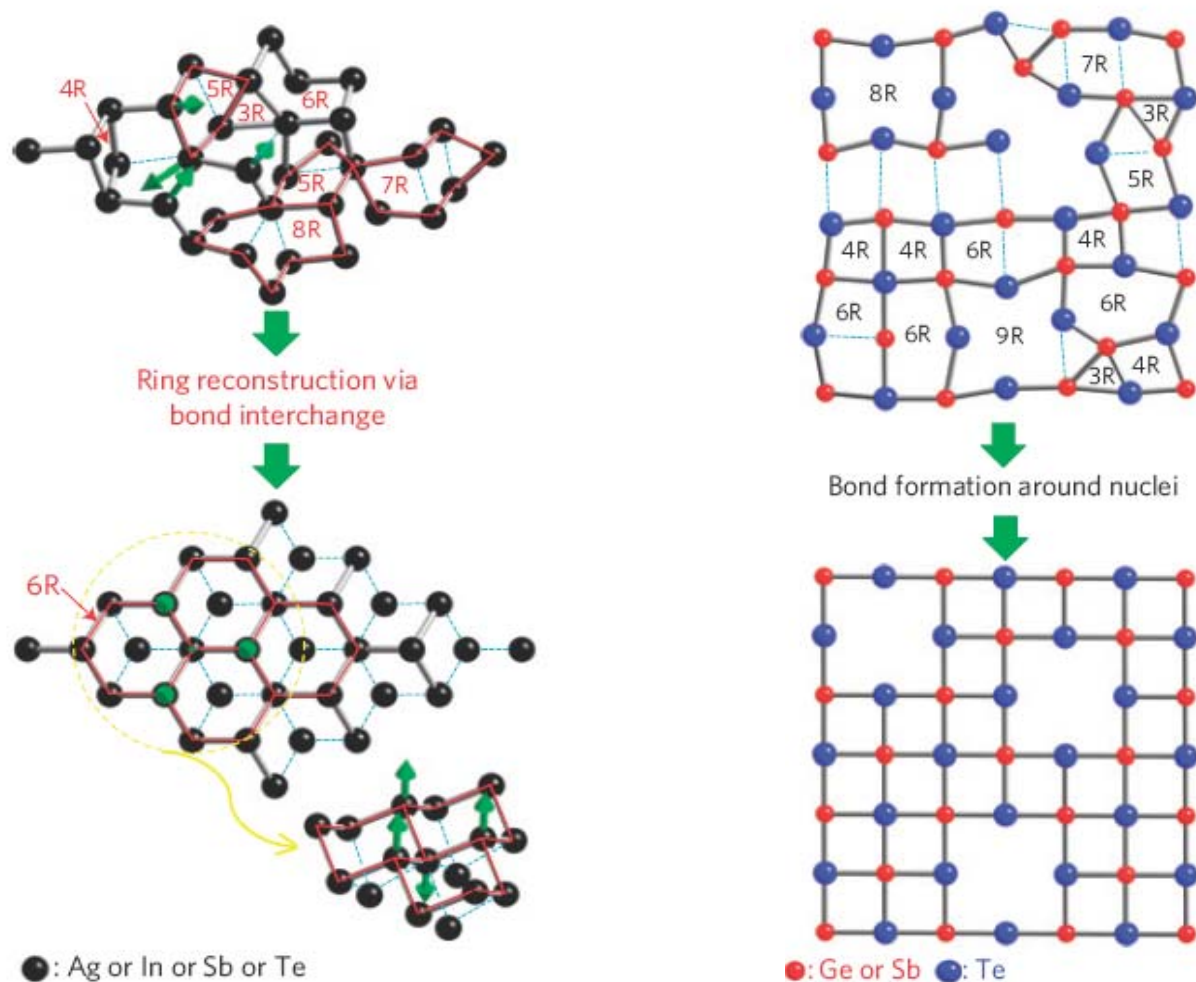
- ✓ The structure of a-AIST shows a range of atomic ring sizes, whereas a-GST shows mainly small rings and cavities.
- ✓ The local environment of Sb in both forms of AIST is a distorted 3+3 octahedron, suggesting a bond-interchange model, where a sequence of small displacements of Sb atoms accompanied by interchanges of short and long bonds is the origin of the rapid crystallization of a-AIST. It differs profoundly from crystallization in a-GST.



The bonding electrons are excited by laser light, causing the atoms in the amorphous phase to move. Finally, the central atom with three short (red) and three long (dashed) bonds crosses the centre of the distorted octahedron, interchanging a short and a long bond.

Amorphous structures proposed

- ✓ A 'bond-interchange' model is proposed as the origin of growth-dominated crystallization of a-AIST, whereas the large fraction of crystalline nuclei in a-GST (embryo nucleation) is the origin of the nucleation-driven crystallization in GST.



Prospects and opportunities

- ✓ Optical memory based on phase change driven by laser irradiation
- ✓ Electrical memory based on phase change driven by electrical field
 - Replacement of Flash memory
 - A nonvolatile DRAM
- ✓ Switch array (logic) based on phase switching
- ✓ Cognitive computing based on phase switching
- ✓ Switch fabric based on threshold switching

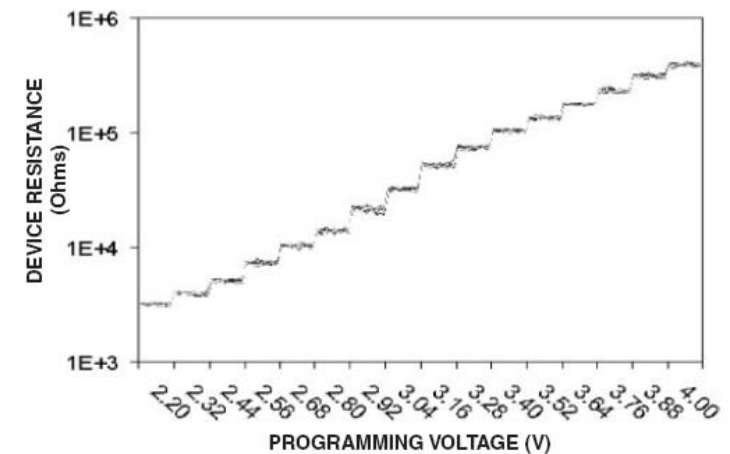
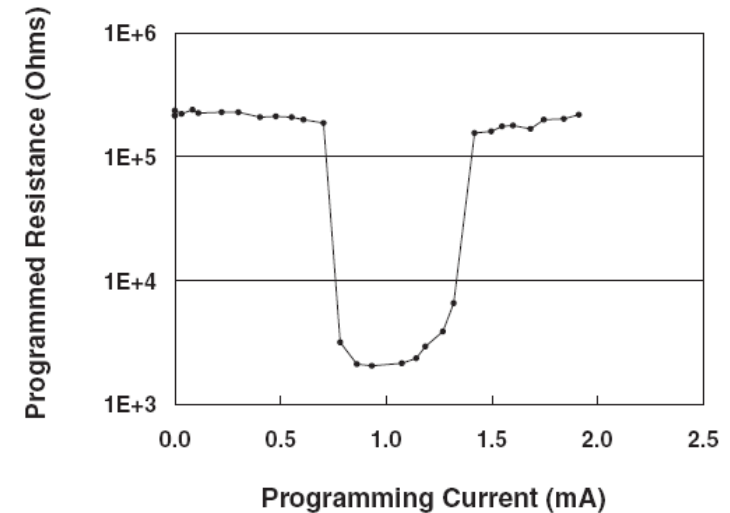
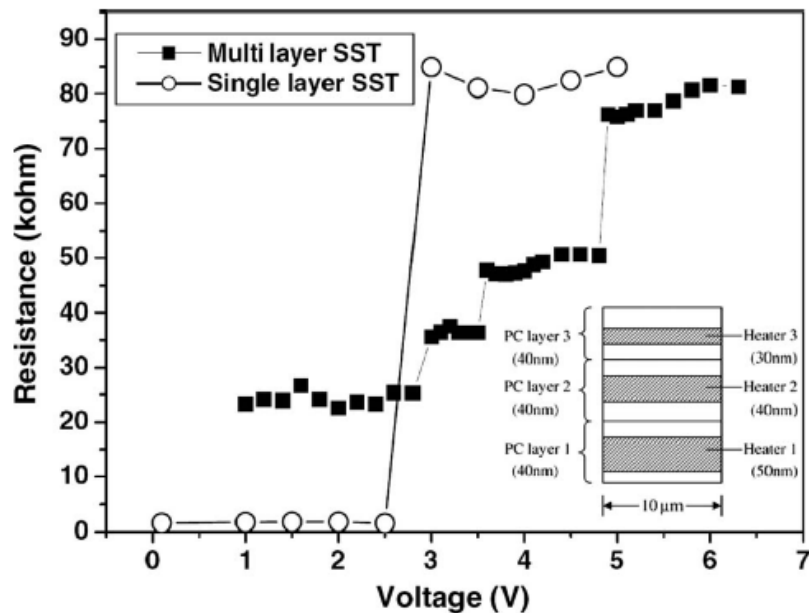


Figure in the left: Zhang et al, Phys. Stat. Sol., Rapid Res. Lett. 1 (2007) R28.
Figures in the right: Ovshinsky, Jap. J. Appl. Phys. 43 (2004) 4695.

Opportunities from the material's viewpoint

- ✓ The amorphous side of the phase change chalcogenides is relatively not known.
 - Lack of good experimental probes for structural analysis
 - Diverse structural parameters reported, sometimes contradictory each other
- ✓ The amorphous side is bottlenecking.
- ✓ Some related questions not clearly answered yet;
 - How and why are the amorphous phases stable despite the fast crystallization?
 - Are the amorphous structures of PCM very different from those of typical ChGs?
 - Can the concepts and languages of traditional ChGs be also applied?
 - What is the origin(s) of threshold switching?
 - What amorphous structure(s) is most suitable as PS or TS materials?
 - What are the traps of charge carriers and their distribution?
 - What about the transport number?
 - What is the new question arising after the existing questions would be answered?